Article

Probing the Coupling between Proton and Electron Transfer in Photosystem II Core Complexes Containing a 3-Fluorotyrosine

Fabrice Rappaport, Alain Boussac, Dee Ann Force, Jeffrey Peloquin, Marcin Brynda, Miwa Sugiura, Sun Un, R. David Britt, and Bruce A. Diner

J. Am. Chem. Soc., **Article ASAP** • DOI: 10.1021/ja808604h • Publication Date (Web): 05 March 2009

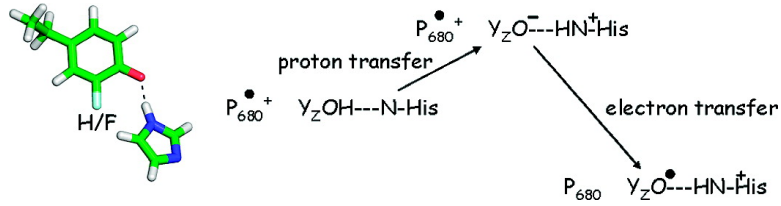

More About This Article

Additional resources and features associated with this article are available within the HTML version:

- Supporting Information
- Access to high resolution figures
- Links to articles and content related to this article
- Copyright permission to reproduce figures and/or text from this article

View the Full Text HTML

J|A|C|S
ARTICLES

Probing the Coupling between Proton and Electron Transfer in Photosystem II Core Complexes Containing a 3-Fluorotyrosine

Fabrice Rappaport,*,† Alain Boussac,‡ Dee Ann Force,§,▽ Jeffrey Peloquin,⊥ Marcin Brynda,|| Miwa Sugiura,¶ Sun Un,‡ R. David Britt,|| and Bruce A. Diner§

Institut de Biologie Physico-Chimique, UMR 7141 CNRS-UPMC, 13 rue Pierre et Marie Curie, 75005 Paris, France, iBiTec-S, URA CNRS 2096, CEA Saclay, 91191 Gif sur Yvette, France, CR&D, Experimental Station, E. I. du Pont de Nemours & Co., Wilmington, Delaware 19880-0173, Department of Chemistry and Biochemistry, Boise State University, Boise, Idaho 83725-1520, Department of Chemistry, University of California, One Shields Avenue, Davis, California 95616-0935, and Cell-Free Science and Technology Research Center, Ehime University Bunkyo-cho, Matsuyama, Ehime 790-8577, Japan

Received November 7, 2008; E-mail: Fabrice.Rappaport@ibpc.fr

Abstract: The catalytic cycle of numerous enzymes involves the coupling between proton transfer and electron transfer. Yet, the understanding of this coordinated transfer in biological systems remains limited, likely because its characterization relies on the controlled but experimentally challenging modifications of the free energy changes associated with either the electron or proton transfer. We have performed such a study here in Photosystem II. The driving force for electron transfer from Tyr_Z to $P_{680}^{\bullet+}$ has been decreased by ~80 meV by mutating the axial ligand of P_{680}, and that for proton transfer upon oxidation of Tyr_Z by substituting a 3-fluorotyrosine (3F-Tyr_Z) for Tyr_Z. In Mn-depleted Photosystem II, the dependence upon pH of the oxidation rates of Tyr_Z and 3F-Tyr_Z were found to be similar. However, in the pH range where the phenolic hydroxyl of Tyr_Z is involved in a H-bond with a proton acceptor, the activation energy of the oxidation of 3F-Tyr_Z is decreased by 110 meV, a value which correlates with the *in vitro* finding of a 90 meV stabilization energy to the phenolate form of 3F-Tyr when compared to Tyr (Seyedsayamdost et al. *J. Am. Chem. Soc.* **2006**, *128*,1569−1579). Thus, when the phenol of Y_Z acts as a H-bond donor, its oxidation by $P_{680}^{\bullet+}$ is controlled by its prior deprotonation. This contrasts with the situation prevailing at lower pH, where the proton acceptor is protonated and therefore unavailable, in which the oxidation-induced proton transfer from the phenolic hydroxyl of Tyr_Z has been proposed to occur concertedly with the electron transfer to $P_{680}^{\bullet+}$. This suggests a switch between a concerted proton/electron transfer at pHs < 7.5 to a sequential one at pHs > 7.5 and illustrates the roles of the H-bond and of the likely salt-bridge existing between the phenolate and the nearby proton acceptor in determining the coupling between proton and electron transfer.

1. Introduction

Many enzymes produce radical intermediates in cycling through their catalytic mechanism. Prominent among these is Photosystem II (PSII) which drives the oxidation of water to dioxygen and supplies our atmosphere with the substrate of aerobic metabolism. In PSII, absorption of a photon leads to the formation of a radical pair, $P_{680}^{\bullet+}Phe^{\bullet-}$, which traps a major part of the photon energy. $P_{680}^{\bullet+}$ is then quickly reduced by Y_Z which is in turn reduced by an electron abstracted from the $(Mn)_4Ca$ cluster.[1−3] Once this sequence is repeated four times, two water molecules are split into O_2, and the enzyme is reset to its lowest oxidation state. Although the overall catalytic mechanism is known at the phenomenological level, the description at the molecular or atomic level still remains a challenge. Beside its academic interest, a molecular description of the sequence of reactions that produce the strongest oxidants known in biological systems[4−6] should help to design artificial compounds that mimic the light-driven splitting of water and which could eventually sustain hydrogen production.[7−9] Although the $(Mn)_4Ca$ cluster is the catalytic center which drives water splitting, the redox cycling of ($Y_ZOH/Y_ZO^{\bullet}$) has received

† Institut de Biologie Physico-Chimique, UMR 7141 CNRS-UPMC.
‡ iBiTec-S, URA CNRS 2096.
§ E. I. du Pont de Nemours & Co.
⊥ Boise State University.
|| University of California - Davis.
¶ Ehime University Bunkyo-cho.
▽ Present address: Department of Chemistry and Biochemistry, Boise State University, Boise, ID, 83725-1520.

(1) Diner, B. A.; Rappaport, F. *Annu. Rev. Plant Biol.* **2002**, *53*, 551–580.
(2) Rappaport, F.; Diner, B. A. *Coord. Chem. Rev.* **2008**, *252*, 259–272.
(3) Dau, H.; Haumann, M. *Coord. Chem. Rev.* **2008**, *252*, 273–295.
(4) Rappaport, F.; Guergova-Kuras, M.; Nixon, P. J.; Diner, B. A.; Lavergne, J. *Biochemistry* **2002**, *41*, 8518–8527.
(5) Cuni, A.; Xiong, L.; Sayre, R. T.; Rappaport, F.; Lavergne, J. *Phys. Chem. Chem. Phys.* **2004**, *6*, 4825–4831.
(6) Grabolle, M.; Dau, H. *Biochim. Biophys. Acta* **2005**, *1708*, 209–218.
(7) Esswein, A. J.; Nocera, D. G. *Chem. Rev.* **2007**, *107*, 4022–4047.
(8) Irebo, T.; Reece, S. Y.; Sjödin, M.; Nocera, D. G.; Hammarström, L. *J. Am. Chem. Soc.* **2007**, *129*, 15462–15464.
(9) Herrero, C.; Lassalle-Kaiser, B.; Leibl, W.; Rutherford, A. W.; Aukauloo, A. *Coord. Chem. Rev.* **2008**, *252*, 456–468.

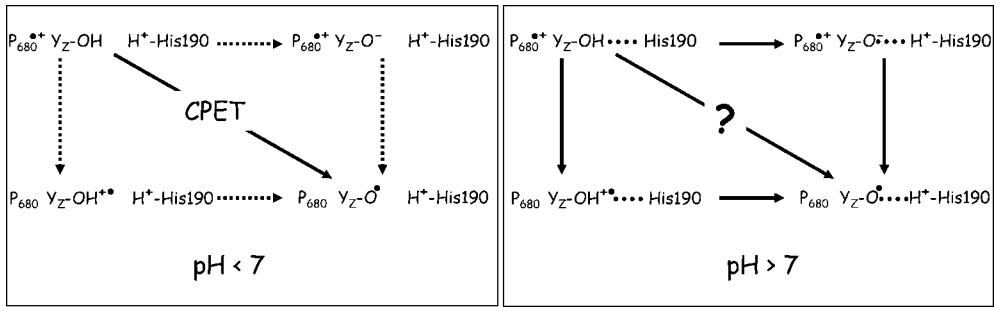

Figure 1. Scheme depicting the reaction pathways for the electron and proton transfer from the phenol group of Y_Z in Mn-depleted PSII. (Left) Situation proposed to prevail at low pH, where the nearby proton-accepting base (shown here as being D_1-His190, see text for a discussion) is protonated and thus unavailable as a proton acceptor. As discussed in the text, the characteristics of the oxidation rate of Y_Z are those expected for a concerted proton/electron transfer (CPET). (Right) Situation thought to prevail above pH ≈ 7, where a proton-accepting base in close vicinity to the phenol group of Y_Z is available. The nature of the coupling between the electron transfer and proton transfer from the phenol group of Y_Z is the subject of the present study.

considerable attention because both the oxidation and reduction of Y_Z are coupled to a proton transfer, making Y_Z^{ox} a likely player in the chemical scenario of the abstraction of four electrons and four protons from the two water molecules.[10−13] Also, as it is amenable to time-resolved study, it serves as a paradigm for understanding the coupling between electron and proton transfer in biomimetic systems.[14−17]

The strongest evidence for tight coupling between electron and proton transfer from Y_Z came from the studies of site-directed PSII mutants lacking the His D_1-190, in which the oxidation of Y_Z was markedly slowed down and could be kinetically rescued by addition of an exogenous proton acceptor.[18−21] This finding, together with Y_Z being protonated in its reduced form[22−24] and Y_Z^{ox} being a neutral radical, raises the question of the reaction pathway followed to abstract both a proton and an electron from the phenol side chain. Efforts to disentangle this pathway have heretofore relied on the study of the dependence of the rate of oxidation of Y_Z on pH[11,21] or on the driving force of the electron-transfer reaction proper.[25] The former approach led to the characterization of two different regimes for the oxidation of Y_Z, depending on the protonation state of the base serving as a proton acceptor from Y_Z^{ox}. Below pH 7, the oxidation of Y_Z in Mn-depleted PSII is slow and has significant activation energy (E_a ≈ 300 meV[11]). The rate can be accelerated by the addition of mobile proton carriers[21] indicating that proton release is kinetically limiting the electron-transfer reaction from Y_Z to $P_{680}^{•+}$. Yet, in this pH range, the rate of oxidation of Y_Z shows a similar dependence on the driving force for either H^+ release or electron transfer, indicating that the overall reaction proceeds by a concerted proton/electron transfer.[25] Above pH ≈ 7, the oxidation rate of Y_Z is increased about 30-fold but only very weakly depends on the driving force for H^+ release, and its activation energy is smaller (E_a ≈ 150 meV[11]). In an artificial complex, the oxidation of a phenol group bound to Ru(II)-polypyridine showed similar characteristics, a strong dependence on pH and a significant activation energy below the pK_a of the phenol group and a weak activation energy and no dependence on pH above the pK_a.[26] In this case, the dependence upon pH of the oxidation rate of the phenol group and its significant activation energy were accounted for by a concerted electron/proton transfer from the phenol, and by analogy, this mechanism was proposed to apply as well in Mn-depleted PSII.[26] Yet, this analogy only holds in the pH range where the oxidation of Y_Z indeed displays similar characteristics, a pH-dependent and significantly activated oxidation rate or in other terms below pH ≈ 7. In addition, whereas in the artificial system the transition between the regime where the oxidation rate of the phenol group depends on pH to the regime where it is pH independent likely reflects the transition from the phenol to the phenolate, in Mn-depleted PSII it is interpreted as reflecting the deprotonation of a nearby proton-accepting base rather than the deprotonation of the phenol group of Y_Z proper.

While, as illustrated in Figure 1, in the absence of this nearby proton-accepting base (i.e., in Mn-depleted PSII and in the low pH range), there is therefore a consensus on the nature of the coupling between the proton and electron transfer from Y_Z, the mechanism by which oxidation of Y_Z proceeds when the nearby base is available as a proton-accepting group at high pH in Mn-depleted PSII remains uncharacterized.

This latter case is particularly important since, in these circumstances, the structural and kinetic characteristics which determine the electron and proton transfers from or to Y_Z more closely correspond to those prevailing when water oxidation is active. Indeed, according to the 3D structure of O_2-evolving PSII, the oxygen of the phenol group of Y_Z is at H-bonding

(10) Rappaport, F.; Blanchard-Desce, M.; Lavergne, J. *Biochim. Biophys. Acta* **1994**, *1184*, 178–192.
(11) Ahlbrink, R.; Haumann, M.; Cherepanov, D.; Bögershausen, O.; Mulkidjanian, A.; Junge, W. *Biochemistry* **1998**, *37*, 1131–1142.
(12) Haumann, M.; Liebisch, P.; Muller, C.; Barra, M.; Grabolle, M.; Dau, H. *Science* **2005**, *310*, 1019–1021.
(13) Renger, G. *Biochim. Biophys. Acta* **2004**, *1655*, 195–204.
(14) Mayer, J. M.; Rhile, I. J.; Larsen, F. B.; Mader, E. A.; Markle, T. F.; DiPasquale, A. G. *Photosynth. Res.* **2006**, *87*, 3–20.
(15) Cukier, R. I.; Nocera, D. G. *Annu. Rev. Phys. Chem.* **1998**, *49*, 337–369.
(16) Lomoth, R.; Magnuson, A.; Sjödin, M.; Huang, P.; Styring, S.; Hammarström, L. *Photosynth. Res.* **2006**, *87*, 25–40.
(17) Markle, T. F.; Rhile, I. J.; Dipasquale, A. G.; Mayer, J. M. *Proc. Natl. Acad. Sci. U.S.A.* **2008**, *105*, 8185–8190.
(18) Diner, B. A.; Nixon, P. J.; Farchaus, J. W. *Curr. Opin. Struct. Biol.* **1991**, *1*, 546–554.
(19) Mamedov, F.; Sayre, R. T.; Styring, S. *Biochemistry* **1998**, *37*, 14245–14256.
(20) Hays, A.-M. A.; Vassiliev, I. R.; Golbeck, J. H.; Debus, R. J. *Biochemistry* **1998**, *37*, 11352–11365.
(21) Hays, A.-M. A.; Vassiliev, I. R.; Golbeck, J. H.; Debus, R. J. *Biochemistry* **1999**, *38*, 11851–11865.
(22) Berthomieu, C.; Hienerwadel, R.; Boussac, A.; Breton, J.; Diner, B. A. *Biochemistry* **1998**, *37*, 10548–10554.
(23) Noguchi, T.; Inoue, Y.; Tang, X.-S. *Biochemistry* **1997**, *36*, 14705–14711.
(24) Berthomieu, C.; Hienerwadel, R. *Biochim. Biophys. Acta* **2005**, *1707*, 51–66.
(25) Diner, B. A.; Bautista, J. A.; Nixon, P. J.; Berthomieu, C.; Hienerwadel, R.; Britt, R. D.; Vermaas, W. F.; Chisholm, D. A. *Phys. Chem. Chem. Phys.* **2004**, *6*, 4844–4850.
(26) Sjödin, M.; Styring, S.; Åkermark, B.; Sun, L.; Hammarström, L. *J. Am. Chem. Soc.* **2000**, *122*, 3932−3936.

distance (2.7 Å) to the ε-N of the imidazole ring of His-190.[27,28] In addition, the time constant of the oxidation of Y_Z lies in the 50−400 ns time range, depending on the oxidation state of the $(Mn)_4Ca$ cluster,[29] a situation which markedly differs from that observed in Mn-depleted PSII below pH 7 but which is close to that reached in Mn-depleted PSII at alkaline pH (ref 21 and this work). Many studies, including infrared and magnetic resonance spectroscopy, support a model in which, in Mn-depleted PSII, both the Y_ZOH and $Y_ZO^•$ states are involved in a H-bond.[22,30,31] These observations, combined with the faster rate for the oxidation of Y_Z at alkaline pH, call for the characterization of the coupling between proton and electron transfer upon Y_Z oxidation under conditions where the H-bond is preserved.

In order to better understand the coordination of the proton and electron transfer, we have changed the driving force for the electron and/or proton transfer and assessed the kinetic consequences of such changes. The driving force for electron transfer proper was modified by site-directed mutagenesis to alter the midpoint potential of P_{680}[32] (by 80 mV), and the driving force for proton transfer was tuned by incorporating a fluorinated tyrosine in place of Y_Z (ΔpK_a 1.5 pH units[33]).

2. Materials and Methods

2.1. Incorporation of 3F-Tyrosine and Purification of PSII Core Complexes. The incorporation of tyrosine which is fluorinated on the carbon 3 of the phenol ring (3F-Tyr) in *Thermosynechococcus elongatus* was performed as described in ref 34. The culture medium was supplemented with 125 μM L-Phe, 125 μM L-Trp, and 125 μM L-3F-Tyr purchased from Sigma-Aldrich. Photosystem II (PSII) core complexes were purified as described in ref 35. Mn-depletion was performed as in ref 36.

Synechocystis Olive WT cells bearing a hexahistidine C-terminal tail on PsbB[37] were grown photoautotrophically in 10 L of BG-11 minimal medium. Once the OD_{730} had reached 0.4−0.5/cm, the medium was supplemented with 0.5 mM 3-F-tyrosine, 0.5 mM phenylalanine, and 0.25 mM tryptophan, added under sterile conditions to bring the volume up to 11 L. The cells were cultivated from 24−72 h under these conditions and harvested in an Amicon DC10 hollow-fiber concentrator. The cells were broken, and the PSII core complexes were isolated as described in ref 37 and concentrated in a Centricon 100 concentrator. The core complexes were treated with 5 mM hydroxylamine for 30 min on ice in 50 mM MES-NaOH, pH 6.5, 5 mM $MgCl_2$, 20 mM $CaCl_2$, 25% glycerol + 0.03% dodecyl maltoside to reduce and extract the manganese cluster, and then applied to an ECONOPAK 10DG gel filtration column equilibrated with the same buffer to remove free Mn^{2+} and residual hydroxylamine.

Synechocystis WT and D1-His198Ala core complexes were isolated from strains described previously.[32] The core complexes were prepared according to the combined procedures of Tang and Diner[38] and Rögner et al.[39] in that order, and were stored at −80 °C until use.

2.2. EPR Spectroscopy. Electron spin echo (ESE)-field-swept spectra where recorded at 4.2 K with a Bruker Elexsys 580 X-band spectrometer equipped with an Oxford Instruments cryostat for *T. elongatus* and at 40 K with a home-built[40] spectrometer for *Synechocystis*. In both cases, a 2-pulse sequence was used with a duration of 48 and 96 ns for the π/2 and π pulses. The τ value was 300 ns. The shot repetition time was 16 ms for *T. elongatus* and 2 ms for *Synechocystis*.

In *T. elongatus*, ferricyanide (5 mM, final concentration) was added to the sample as an artificial electron acceptor. The D1 subunit Tyr-161 radical ($Y_Z^•$) was induced by illumination of the Mn-depleted PSII at −40 °C for 5 s. Then, the samples were immediately transferred in the dark to 198 K and then to 77 K. Illumination of the samples was performed in a nonsilvered Dewar flask filled with ethanol and cooled to −40 °C with liquid N_2. The light source was an 800-W tungsten lamp, light from the beam of which was filtered through water and IR filters. The $Y_Z^•$ component of the spectrum recorded after illumination was obtained by subtracting the $Y_D^•$ spectrum recorded after thawing the sample in the dark at which point the $Y_Z^•$ signal rapidly decays.

Synechocystis PSII samples were loaded into EPR tubes with 300 μM $K_3Fe(CN)_6$. $Y_Z^•$ and $Y_D^•$ were trapped together by freezing under illumination (∼5000 W/m^2) in ≤20 s above a pool of liquid N_2 contained in a transparent Dewar. $Y_D^•$ alone was recorded after a further dark-adaptation for 15 min on ice which relaxes $Y_Z^•$. The sample was then frozen in the dark in liquid N_2 prior to recording the ESE field-swept spectra.

2.3. Time-Resolved Absorption Spectroscopy. Absorption changes were measured using a laboratory-built spectrophotometer described in ref 41. The PSII core complexes were resuspended at a chlorophyll concentration of 25 μg/mL in a medium containing 10 mM $CaCl_2$, 10 mM $MgCl_2$, and 50 mM of the appropriate buffer (2-(*N*-morpholino)ethanesulfonic acid (MES) for the 5.0−6.5 pH range, 4-(2-hydroxyethyl)-1-piperazine ethanesulfonic acid (HEPES) for the 7.0−8.5 pH range, and *N*-cyclohexyl-2-aminoethanesulfonic acid (CHES) for the 8.5−10.5 pH range). 2,6 Dichloro-*p*-benzoquinone (100 μM) was added as an electron acceptor. The temperature of the cuvette was controlled by a thermostatted circulating bath.

3. Results

Two different strategies can be followed for substituting an exogenous 3F-Tyr for a Tyr. In the case of the ribonucleotide reductase, the specific substitution of a single Tyr residue in the entire protein was achieved through purification, cleavage, and fusion with a synthetic peptide containing a F-Tyr.[42] PSII being a membrane protein comprising more than 20 subunits such an elegantly targeted strategy was unrealistic, and we resorted to a global labeling approach as in refs 43 and 44 in the thermophilic organism *T. elongatus* and mesophilic organism *Synechocystis* sp. PCC 6803. We thus first assessed the

(27) Ferreira, K. N.; Iverson, T. M.; Maghlaoui, K.; Barber, J.; Iwata, S. *Science* **2004**, *303*, 1831–1838.
(28) Loll, B.; Kern, J.; Saenger, W.; Zouni, A.; Biesiadka, J. *Nature* **2005**, *438*, 1040–1044.
(29) Brettel, K.; Schlodder, E.; Witt, H. T. *Biochim. Biophys. Acta* **1984**, *766*, 403–415.
(30) Diner, B. A.; Force, D. A.; Randall, D. W.; Britt, R. D. *Biochemistry* **1998**, *37*, 17931–17943.
(31) Force, D. A.; Randall, D. W.; Britt, R. D.; Tang, X. S.; Diner, B. A. *J. Am. Chem. Soc.* **1995**, *117*, 12643–12644.
(32) Diner, B. A.; Schlodder, E.; Nixon, P. J.; Coleman, W. J.; Rappaport, F.; Lavergne, J.; Vermaas, W. F.; Chisholm, D. A. *Biochemistry* **2001**, *40*, 9265–9281.
(33) Seyedsayamdost, M. R.; Reece, S. Y.; Nocera, D. G.; Stubbe, J. *J. Am. Chem. Soc.* **2006**, *128*, 1569–1579.
(34) Boussac, A.; Verbavatz, J. M.; Sugiura, M. *Photosynth. Res.* **2008**, *98*, 285–292.
(35) Sugiura, M.; Boussac, A.; Noguchi, T.; Rappaport, F. *Biochim. Biophys. Acta* **2008**, *1777*, 331–342.
(36) Un, S.; Boussac, A.; Sugiura, M. *Biochemistry* **2007**, *46*, 3138–3150.
(37) Lakshmi, K. V.; Reifler, M. J.; Chisholm, D. A.; Wang, J. Y.; Diner, B. A.; Brudvig, G. W. *Photosynth. Res.* **2002**, *72*, 175–189.
(38) Tang, X.-S.; Diner, B. A. *Biochemistry* **1994**, *33*, 4594–4603.
(39) Rögner, M.; Nixon, P. J.; Diner, B. A. *J. Biol. Chem.* **1990**, *265*, 6189–6196.
(40) Sturgeon, B. E.; Ball, J. A.; Randall, D. W.; Britt, R. D. *J. Phys. Chem.* **1994**, *98*, 12871–12883.
(41) Beal, D.; Rappaport, F.; Joliot, P. *Rev. Sci. Instrum.* **1999**, *70*, 202–207.
(42) Seyedsayamdost, M. R.; Stubbe, J. *J. Am. Chem. Soc.* **2006**, *128*, 2522–2523.

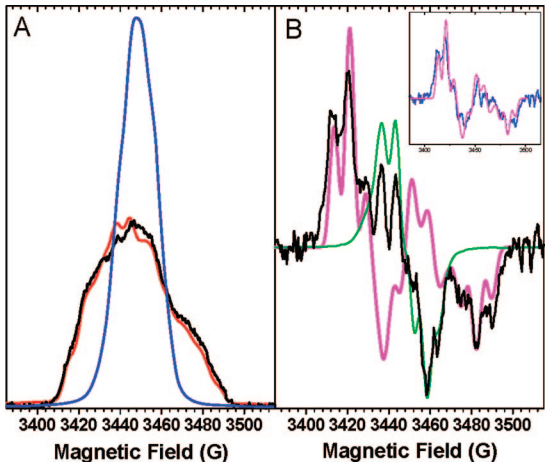

Figure 2. (A) ESE field-swept difference spectra of labeled PSII core complexes from *T. elongatus* (black) and *Synechocystis* sp. PCC 6803 (red) and of unlabeled PSII core complexes from *T. elongatus* (blue). All spectra have been normalized to an area of one spin. (B) Comparison between the first derivative of the ESE field-swept spectrum of labeled PSII core complexes from *T. elongatus* (black) with the simulated spectrum of 3F-$Y_Z^{\bullet}$ (magenta). Shown in green is the spectrum of $Y_Z^{\bullet}$ scaled to account for 25% of the total spin number in the experimental spectrum. The inset compares the difference between the experimental spectrum and the scaled spectrum of $Y_Z^{\bullet}$ (blue) to the simulated spectrum (magenta).

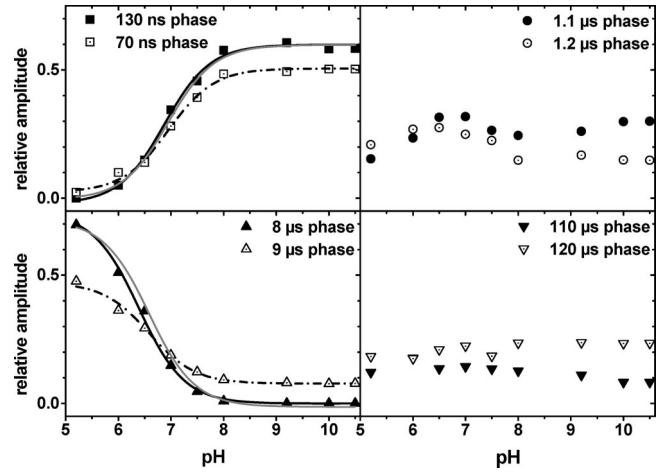

Figure 3. Relative amplitudes of the four exponentials components associated with the reduction of $P_{680}^{\bullet+}$ as a function of pH. The reduction of $P_{680}^{\bullet+}$ was measured at 432 nm from 5 ns to 10 ms at various pHs, and the kinetics were globally fit with four exponentials (the half-times of which are indicated in the different panels). The solid symbols correspond to the unlabeled PSII from *T. elongatus*. Fitting these data (solid lines) with the Henderson−Haselbach equation ($n = 1$) yielded pK_a's of 6.85 ± 0.15 and 6.4 ± 0.2 for the 130 ns and 8 μs components, respectively. The open symbols correspond to the labeled PSII from *T. elongatus*. Fitting these data (dashed lines) with the Henderson−Haselbach equation ($n = 1$) yielded pK_a's of 6.9 ± 0.2 and 6.55 ± 0.3 for the 70 ns and 9 μs components, respectively. The solid lines in gray are the fit of the data obtained with labeled PSII normalized to the data obtained with the unlabeled PSII to facilitate the comparison.

incorporation yield of the 3F-Tyr by EPR, which allows one to probe specifically the redox active tyrosines in the protein.

Figure 2A compares the electron spin echo (ESE) field-swept-EPR difference spectra of Mn-depleted PSII core complexes from 3F-$Y_Z^{\bullet}$ *T. elongatus* and *Synechocystis* with that from unlabeled *T. elongatus*.

These spectra were generated by first recording the ESE-field swept spectra of $Y_Z^{\bullet}$ and $Y_D^{\bullet}$ and then subtracting the ESE-field swept spectra of $Y_D^{\bullet}$. First it is clear that the incorporation of 3F-Tyr leads to a significant broadening of the spectra from both organisms. Second, it is also clear that the 3F-$Y_Z^{\bullet}$ spectra are of similar amplitude, indicating an equivalent extent of incorporation of the fluorinated tyrosine into both organisms. Figure 2B shows the ESE field-swept spectrum of the (3F)-$Y_Z^{\bullet}$ radical in PSII from *T. elongatus* (black) after a pseudomodulation has been applied. When referring specifically to the fluorinated Y_Z or to the nonfluorinated Y_Z, we will use the notation 3F-Y_Z and Y_Z, respectively. (3F)-Y_Z will be used when referring without distinction to the fluorinated or nonfluorinated Y_Z. To quantify the yield of the incorporation, the simulated spectrum of 3F-$Y_Z^{\bullet}$ (magenta, see the Supporting Information for details) was scaled to match the spectral patterns of the external "wings", diagnostic of the large hyperfine splitting due to the presence of the ^{19}F nucleus and absent in the unlabeled $Y_Z^{\bullet}$ radical (shown in green). The comparison of the integrated areas of the scaled 3F-$Y_Z^{\bullet}$ simulated spectrum with the experimental one sets the percent of 3F-Tyr incorporation at 75 ± 5% for *T. elongatus*. As shown in the inset of Figure 2B the difference between the ESE field-swept spectrum of (3F)-$Y_Z^{\bullet}$ radical and of unlabeled $Y_Z^{\bullet}$, scaled to an area of 0.25 spin (blue spectrum), nicely matches the simulated spectrum of 3F-$Y_Z^{\bullet}$ (magenta).

The consequence of the substitution on the rate of oxidation of 3F-Y_Z was then characterized. We studied the pH dependence of the kinetics of $P_{680}^{\bullet+}$ reduction in labeled and unlabeled PSII from *T. elongatus*. These were followed at 432 nm where the oxidation of P_{680} is associated with a strong bleaching band. The reduction of $P_{680}^{\bullet+}$ in *T. elongatus* was well fit with four exponential decays as found earlier by Hays et al. in *Synechocystis* sp. PCC 6803[21] (see Figure S2 in the Supporting Information). The amplitude of the individual decay components varied with pH, whereas the individual rate constants were rather pH insensitive as also found earlier in *Synechocystis* sp. PCC 6803.[21] We thus globally fit the various kinetic components obtained at different pHs using four pH-independent rate constants. The amplitude of each of these four components as a function of pH is shown in Figure 3. Two main conclusions can be drawn. The overall pH dependence of $P_{680}^{\bullet+}$ reduction is similar in *T. elongatus* and *Synechocystis* PSII. Indeed, as in the *Synechocystis* case (see Figure 4 of Hays et al.[21]), the amplitudes of the first and third components are those which more strongly depend on pH, and their dependencies are, to a first approximation, complementary. Even more saliently, the substitution of 3F-Y_Z for Y_Z had hardly any effect on the pH dependence of the kinetics of reduction of $P_{680}^{\bullet+}$. Again, the first and third components were those displaying the more pronounced pH dependence, and although the maximum amplitudes were slightly smaller in the labeled cases, the pK_a's characterizing the pH dependencies of each component were similar to those observed with unlabeled PSII.

The kinetic complexity found here for the reduction of $P_{680}^{\bullet+}$ in Mn-depleted PSII core complexes from *T. elongatus* nicely reproduces previous results from different groups,[11,20,21,45] and

(43) Barry, B. A.; Babcock, G. T. *Proc. Natl. Acad. Sci. U.S.A.* **1987**, *84*, 7099–7103.
(44) Ayala, I.; Perry, J. J.; Szczepanski, J.; Tainer, J. A.; Vala, M. T.; Nick, H. S.; Silverman, D. N. *Biophys. J.* **2005**, *89*, 4171–4179.
(45) Conjeaud, H.; Mathis, P. *Biochim. Biophys. Acta* **1980**, *590*, 353–359.

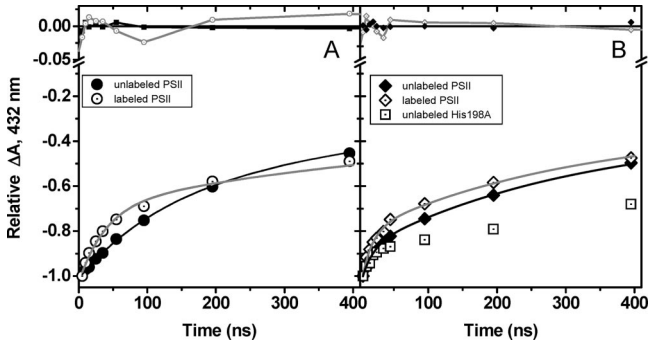

Figure 4. Comparison of the reduction kinetics of $P_{680}^{\bullet+}$ at pH 9.2 in unlabeled (solid symbols) and labeled (open symbols) PSII complexes from *T. elongatus* (left panel) and *Synechocystis* sp. PCC 6803 (right panel) at 15 °C. The kinetics were normalized to their initial amplitude. The lines show the best fit of the data with four exponentials (the gray and black lines correspond respectively to the labeled and unlabeled PSII complexes). The fit yielded the following time constants for the fast component: *T. elongatus*: $1.3 \times 10^7\ s^{-1} \pm 1.5 \times 10^6$ (unlabeled), $2.8 \times 10^7\ s^{-1} \pm 2.2 \times 10^6$ (labeled); *Synechocystis*: $1.9 \times 10^7\ s^{-1} \pm 2.4 \times 10^6$ (unlabeled), $3.7 \times 10^7\ s^{-1} \pm 2.5 \times 10^6$ (labeled), H198A $2.1 \times 10^7 s^{-1} \pm 3.1 \times 10^6$.

discussing the assignment of the different components is beyond the scope of the present study. Briefly, whereas the fast component is commonly assigned to the coupled electron/proton transfer from Y_ZOH, the subsequent components are commonly understood as reflecting the relaxation of the protein moiety and as such are kinetically controlled by local structural rearrangement such as proton transfer or formation of H-bonds. Since the aim of this study was to investigate the nature of the coupling between proton and electron transfer from (3F)-Y_Z, we focused on the fast component. In addition, since we were particularly interested in dissecting these processes under conditions which kinetically resemble those prevailing in oxygen-evolving PSII, we focused our analysis on the high pH range where the proton acceptor is deprotonated and thus the phenol hydroxyl group is thought to be a H-bond donor. Figure 4 shows that, in labeled PSII, the fast component of the reduction of $P_{680}^{\bullet+}$ (in the hundreds of nanoseconds time-range), at pH 9.2, is slightly but significantly faster than in unlabeled PSII. This observation holds true in both the *T. elongatus* and *Synechocystis* species. As such a rate increase may stem from a change in the driving force for electron and/or proton transfer, we also compared the rate of reduction of $P_{680}^{\bullet+}$ in unlabeled but mutated PSII in which the driving force for electron transfer between Y_Z and $P_{680}^{\bullet+}$ has been specifically modified.

A collection of PSII mutants has been described in which the axial His ligand to the P_{680} chlorophyll was replaced by other amino acids.[32] We chose the D1-His198A mutant, in which the midpoint potential of the $P_{680}^{\bullet+}/P_{680}$ couple is downshifted by ~80 mV,[32] a change which qualitatively corresponds to that resulting from the 3F-Tyr labeling since, according to *in vitro* studies, the fluorination induces an upshift of the (3F)-YO$^{\bullet}$/(3F)-YO^{-} midpoint potential by ~60 mV[33] (but see below). Figure 4B shows the kinetics of reduction of $P_{680}^{\bullet+}$ in labeled, unlabeled WT and unlabeled D1-His198A PSII from *Synechocystis* sp. PCC 6803. (We did not perform this experiment with *T. elongatus* PSII since, in this species, the D1-His198 mutations hardly affected the redox properties of P_{680}.[34]) The rate was similar in the mutant and unlabeled PSII (compare the initial slope of the absorption changes in Figure 4) but slightly faster in the labeled PSII. Thus, a decrease in the midpoint potential of the $P_{680}^{\bullet+}/P_{680}$ couple does not produce a change in the reduction rate of $P_{680}^{\bullet+}$. We conclude that a change in the

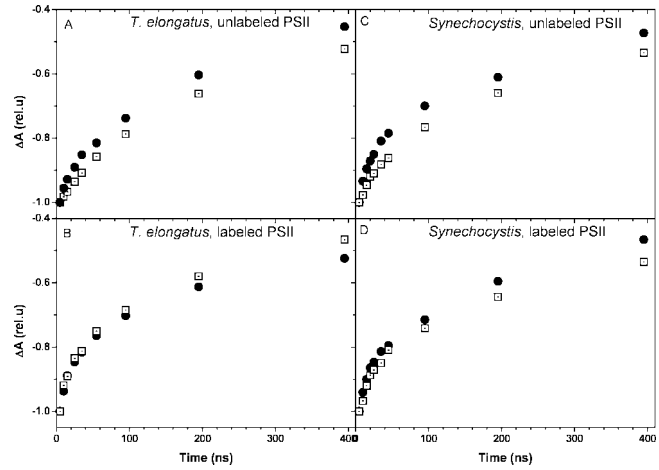

Figure 5. Consequences of the substitution of 3F-Y_Z for Y_Z on the dependence upon temperature of the fast component in the reduction of $P_{680}^{\bullet+}$, at pH 9.2. The left column shows the reduction of $P_{680}^{\bullet+}$ in the hundreds of nanoseconds time range in the unlabeled (panel A) and labeled (panel B) PSII core complexes from *T. elongatus*. The solid circles and open squares show the kinetics at 25−28 and 5 °C, respectively. The right column shows the reduction of $P_{680}^{\bullet+}$ in the hundreds of nanoseconds time range in the unlabeled (panel C) and labeled (panel D) PSII core complexes from *Synechocystis*. The solid circles and open squares depict the kinetics at high and low temperature, respectively. Note that the ordinate axis does not go to 0 and that the figure is a focus on the early events. The fit yielded the following time constants for the fast component: *T. elongatus*: (panel A, unlabeled) $1.75 \times 10^7\ s^{-1} \pm 1.7 \times 10^6$ at 25 °C and $1.05 \times 10^7\ s^{-1} \pm 1.8 \times 10^6$ at 5 °C; (panel B, labeled) $3.2 \times 10^7\ s^{-1} \pm 4.2 \times 10^6$ at 25 °C and $3.1 \times 10^7\ s^{-1} \pm 4.5 \times 10^6$ at 5 °C; *Synechocystis*: (panel C, unlabeled) $3.7 \times 10^7\ s^{-1} \pm 5.7 \times 10^6$ at 28 °C and $1.3 \times 10^7\ s^{-1} \pm 5.8 \times 10^6$ at 5 °C, (panel D, labeled) $5.2 \times 10^7\ s^{-1} \pm 8.2 \times 10^6$ at 28 °C and $3.1 \times 10^7\ s^{-1} \pm 7.5 \times 10^6$ at 5 °C.

driving force for electron transfer from Y_Z to $P_{680}^{\bullet+}$ cannot be the explanation for the acceleration of $P_{680}^{\bullet+}$ reduction produced by tyrosine fluorination.

However, the decrease in the midpoint potential of the $P_{680}^{\bullet+}/P_{680}$ couple qualitatively correlates with a decreased equilibrium constant for the $Y_ZP_{680}^{\bullet+}$ to $Y_Z^{ox}P_{680}$ reaction, as the amplitude of the fast phase was almost halved in the mutant. In the case of the labeled WT PSII, the amplitude of the fast component was diminished by only ~10% (see Figures 3 and 4A), indicating that the substitution with 3F-Tyr only modestly affects the driving force of the electron-transfer reaction.

We further investigated this difference in the overall oxidation rate of (3F)-Y_Z by measuring its temperature dependence in the labeled and unlabeled PSII core complexes from both *Synechocystis* and *T. elongatus*. As shown in Figure 5, the fast component in the reduction of $P_{680}^{\bullet+}$ in the labeled samples was more weakly dependent on the temperature than in the unlabeled samples.

However, in the labeled PSII, this lesser dependence of the rate of reduction of $P_{680}^{\bullet+}$ on temperature does not stem from a smaller driving force for electron transfer. Indeed, as shown in Figure 6, the qualitative comparison of the dependence on the temperature of the kinetics of reduction of $P_{680}^{\bullet+}$ in PSII core complexes from *Synechocystis* WT and D_1-H198A mutant shows that decreasing the driving force for the electron transfer does not result in a weaker temperature dependence.

To further characterize the consequences of the substitution of 3F-Y_Z for Y_Z the temperature dependence of each of the four components was determined. We found that the activation enthalpy of the fast component of the oxidation of Y_Z is larger than that of the oxidation of 3F-Y_Z in both organisms (Figure

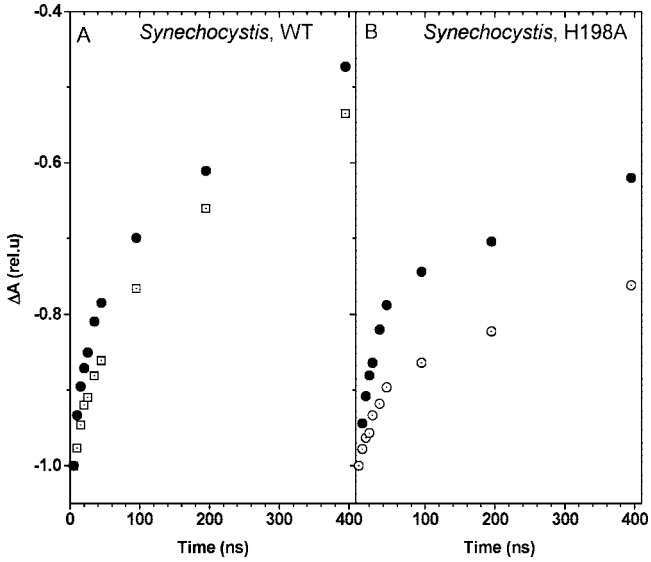

Figure 6. Consequences of the D_1-H198A mutation on the dependence upon temperature of the fast component in the reduction of $P_{680}^{\bullet+}$, at pH 9.2. (Left) Reduction of $P_{680}^{\bullet+}$ in the hundreds of nanoseconds time range in the unlabeled PSII core complexes from *Synechocystis* WT. (Right) Reduction of $P_{680}^{\bullet+}$ in the hundreds of nanoseconds time range in the unlabeled PSII core complexes from *Synechocystis* D_1- H198A mutant. Solid symbols, 25 °C; open symbols, 5 °C. Note that the ordinate axis does not go to 0 and that the figure is a focus on the early events.

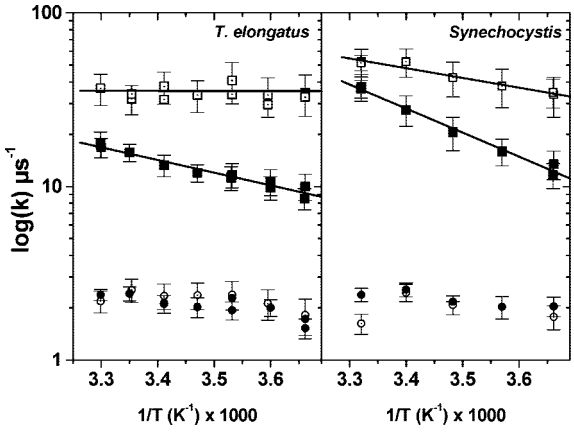

Figure 7. Arrhenius plot of the rates of the first (square) and second component (circle) in the reduction of $P_{680}^{\bullet+}$ at pH 9.2, in unlabeled (solid symbols) and labeled (open symbols) PSII complexes from *T. elongatus* (left panel) and *Synechocystis* sp. PCC 6803 (right panel). The data were linearly fit to extract the activation energy (the results are shown as the solid lines), and the fit yielded the following values: *T. elongatus*: 120 ± 30 meV (unlabeled PSII), 0 ± 25 meV (labeled PSII); *Synechocystis*: 220 ± 35 meV (unlabeled PSII) and 110 ± 25 meV (labeled PSII).

7). Although in *Synechocystis* PSII the activation enthalpy of the oxidation of Y_Z was larger than in *T. elongatus* PSII (220 ± 35 meV and 120 ± 10 meV, respectively), the changes in activation enthalpy resulting from the fluorination were similar, ~110 meV.

4. Discussion

4.1. pH Dependence of the Oxidation of Y_Z and pK_a of Y_ZOH. As the substitution of 3F-Y_Z for Y_Z is expected to decrease the pK_a of the phenol group by 1.5 pH unit,[33] the present results provide an unambiguous way to address two correlated issues: the rationale(s) for the pH dependence of the oxidation of Y_Z in Mn-depleted PSII, as well as the pK_a of Y_Z. The similarity of the dependence on pH of the reduction of $P_{680}^{\bullet+}$ in labeled and unlabeled PSII shows that they reflect the protonation of an amino acid other than Y_Z. The absence of marked differences in the pH dependence of the reduction of $P_{680}^{\bullet+}$ in the pH range extending from 5.2 to 10.5 suggests that the pK_a of 3F-Y_ZOH is larger than 10.5; thus, the apparent pK_a of Y_ZOH would be larger by 1.5 pH units, i.e. ≥12.0.

The mechanistic model which follows from the present data is consistent with the current views on the role of H^+ transfer in determining the overall rate constant for the oxidation of Y_Z.[11,13,21,25,46,47] In the alkaline pH range, the phenol proton of Y_Z would be involved in a H-bond network, with the ε-N of the imidazole ring of His-190 acting as a direct or indirect H^+ acceptor. This network facilitates the deprotonation of Y_ZOH and allows fast electron transfer to $P_{680}^{\bullet+}$. Below pH ≈ 7 the protonation of the H-bond acceptor (likely the ε-N of the imidazole ring) perturbs this H-bond network and the oxidation of Y_Z, proceeding via a concerted proton/electron transfer, is significantly slowed down. Although supporting in essence a similar mechanism, the present results provide further insights into the energetics of the H-bond network in which Y_ZOH is involved. Indeed, based upon the acceleration of the oxidation of Y_Z above pH 9 in a mutant lacking D1-His190, Hays et al. concluded that the pK_a of Y_Z is 10.3 in this mutant.[21] The difference between this previous estimate and the present one (pK_a ≥ 12.0) likely stems from differences in the H-bonded status of the Y_Z phenol group in the two studies. Indeed, the present data were obtained in the presence of D1-His190 the ε-N of which is likely involved, directly or indirectly, in a H-bond with Y_Z (in the following we will denote this H-bond network as Y_ZOH---NHis, with no assumption as to whether D_1-His190 is directly or indirectly H-bonded). This H-bond should stabilize the singly protonated state of the Y_ZOH---NHis ensemble because its deprotonation requires the prior rupture of the H-bond (e.g., ref [17]), and would thus induce an upshift of the apparent pK_a of the Y_ZOH---NHis ensemble. Accordingly, the H-bond would account for the different pK_a for Y_Z in both studies, and this difference would provide an estimate of its strength: $E_H \cong (12.0-10.3) \times 60 \geq 105$ meV, which is in the range corresponding to a H-bond of moderate to significant strength.

4.2. Mechanism of (3F)-Y_Z Oxidation. The study of the fastest component in the reduction of $P_{680}^{\bullet+}$ at pH 9.5 shows the following: (1) it is accelerated by the fluorination of the phenol group of Y_Z, (2) the fluorination results in a decrease of its activation energy by about 110 meV, a value which nicely matches the difference in free energy of deprotonation between 3F-$Y_Z O^-$ and $Y_Z O^-$ as derived from the pK_a shift of 1.5 pH units (90 meV) induced by the fluorination.[33] Although this correlation strongly suggests that the oxidation of Y_Z requires its prior deprotonation, we will first discuss the possibility that the kinetic effect of the fluorination reflects a change in the driving force for electron transfer rather than for proton transfer.

4.3. Dependence of the Rate of Oxidation of Y_Z on the Driving Force for Electron Transfer. A first argument against a hypothesis which asserts that the kinetic consequences of the fluorination would reflect a change in the driving force for electron transfer comes from the electrochemical properties of

(46) Rappaport, F.; Lavergne, J. *Biochim. Biophys. Acta* **2001**, *1503*, 246–259.
(47) Diner, B. A.; Britt, R. D. In *Photosystem II: The Light Driven Water: Plastoquinone Oxidoreductase*; Wydrzynski, T. J., Satoh, K. , Eds.; Springer: Dordrecht, 2005, pp 207−233.

Scheme 1. Stepwise Proton Transfer/Electron Transfer Pathway

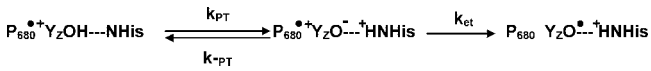

3F-Tyr. Indeed, despite the 63 mV difference between the E_m's of the (3F-YO$^{\bullet}$/3F-YO^{-}) and (YO$^{\bullet}$/YO^{-}) couples, the E_m's of the (3F-YO$^{\bullet}$/3F-YOH) and (YO$^{\bullet}$/YOH) couples are similar (within 20 mV, at most; see Figure 4 in[33]). This similarity stems from the down-shift of the pK_a of the phenol group induced by the fluorination[33] which compensates for the difference in E_m. Thus, the substitution of 3F-Y_Z for Y_Z is not expected to result in a significant change in the driving force for the oxidation of (3F)-Y_Z, since as discussed above, (3F)-Y_Z is protonated when reduced and neutral when oxidized so that, irrespective of the mechanistic pathway, the relevant redox couple is, on thermodynamic grounds, ((3F)-YO$^{\bullet}$/(3F)-YOH). As regards this issue, the amplitude of the fast component of the reduction of $P_{680}^{\bullet+}$ proved to be a sensitive measure of the driving force. It was significantly decreased in the D1-His198A mutant, which induces a down-shift by ~80 mV of the midpoint potential of the $P_{680}^{\bullet+}/P_{680}$ couple.[32] The similar amplitudes observed in the labeled and unlabeled PSII thus show that, as expected, the driving force for electron transfer is hardly affected by the fluorination and that, given the respective electrochemical properties of (3F)-Y_ZOH and (3F)-Y_ZO^{-}, it is (3F)-Y_ZOH that is the electron donor to $P_{680}^{\bullet+}$.

In addition, we found that, in the unlabeled PSII, the oxidation of Y_Z is slightly activated ($\Delta H_a \approx 110$ meV and ≈ 220 meV in *T. elongatus* and *Synechocystis*, respectively), consistent with previous reports of an activation enthalpy of 150 meV for Mn-depleted PSII at pH 9 from pea,[11] or of 100−250 meV in O_2-evolving PSII.[48,49] Yet, a smaller driving force for the electron-transfer reaction due to the lowering of the midpoint potential of the electron acceptor in the D_1-H198A PSII mutant did not weaken the dependence upon temperature of the reduction of $P_{680}^{\bullet+}$ (Figure 5). Thus, the decrease in the activation enthalpy induced by the substitution of 3F-Y_Z for Y_Z cannot result from a change in the driving force for electron transfer for the following two reasons: first, this substitution is not expected to alter this driving force, and second, were it to do so, it would not decrease the activation energy.

4.4. Dependence of the Rate of Oxidation of Y_Z on the Driving Force for Proton Transfer. The question remains as to whether the kinetic effect of the fluorination on the fast component of $P_{680}^{\bullet+}$ reduction can be accounted for by a change in pK_a of (3F)-Y_ZOH. Since the fluorination induces a decrease of the pK_a,[33] the transfer of the phenol proton to a nearby acceptor should be more favorable. This increased driving force for proton transfer should facilitate the formation of the (3F)-YO^{-} species which, in turn, is a more rapid electron donor than (3F)-YOH; thus, the fluorination would be expected to speed up the reduction of $P_{680}^{\bullet+}$, as observed here. Accordingly, the coupled transfer of a proton and an electron from Y_ZOH would follow (Scheme 1).

Yet, the translation of these views into their formal expression has often led to their rebuttal. In such a model, which implicitly assumes that the overall oxidation is kinetically controlled by the deprotonation of the phenol, the apparent rate constant for the oxidation of (3F)-Y_Z is:

$$k_{app} = k_{et} \times \frac{K_H}{1 + K_H} \quad (1)$$

where k_{et} is the intrinsic rate constant of the tyrosinate oxidation and K_H is the equilibrium constant between the (3F)-Y_ZOH---NHis and (3F)-Y_ZO^{-}---HN^{+}His states.

This model has often been discounted because K_H was assumed to be equal to $10^{\Delta pK_a}$, where ΔpK_a is the difference between the pK_a's of the proton acceptor (here, NHis) and the proton donor (here, Y_ZOH). Were this latter assumption to apply, the estimated pK_a of 10.3−12 for Y_Z and 7−7.5 for His190 would yield $k_{app} \cong 10^{-3} \times k_{et}$, and for k_{app} to be $\sim 10^7$ s^{-1}, k_{et} would need to be in the 10^{10} s^{-1} range, a value which is hard to reconcile with the ~10 Å separating the electron donor and acceptor (Y_Z, and $P_{680}^{\bullet+}$, respectively).[26,50−52] Yet, as argued on thermodynamic grounds[46] and on experimental grounds,[53] the salt bridge between the phenolate and the imidazolium in the (3F)-Y_ZO^{-}---HN^{+}His state could affect the coupling between proton and electron transfer with contributions from the electrostatic potentials or electronic coupling arising from the charge distribution. In other words, K_H may differ from $10^{\Delta pK_a}$ as soon as the proton transfer between the H^{+} donor and acceptor results in the possible formation of a salt bridge as in the (3F)-Y_ZO^{-}---HN^{+}His case (we note that this holds as long as the proton acceptor is positively charged when protonated, as would be the case if it were a water molecule or an imidazolium ion). Interestingly, if one assumes that the intrinsic rate constant for electron transfer from (3F)-Y_ZO^{-}---HN^{+}His is temperature independent in the narrow temperature range studied here, the free energy change associated with the transition between (3F)-Y_ZOH---NHis and (3F)-Y_ZO^{-}---HN^{+}His should correspond to the activation energy of the overall reaction, provided the proton transfer along the H-bond is not associated with a significant change in entropy. The above model thus predicts that, provided the strength of the salt bridge is unaltered upon the (3F-Tyr)/Tyr substitution (see the Supporting Information for an experimental support to this assumption), a variation of the pK_a of the proton donor should induce a similar variation of the activation enthalpy. This expectation is satisfyingly met, since in both the *T. elongatus* and *Synechocystis* cases the 3F-Tyr/Tyr substitution resulted in a decrease of the activation enthalpy by ~110 meV which compares favorably to the 90 meV change expected from the difference in pK_a. We thus conclude that (1) there is no strong theoretical reason to dismiss the reaction path through which the electron transfer to $P_{680}^{\bullet+}$ proceeds from the (3F)-Y_ZO^{-}---HN^{+}His state, the relative steady-state concentration of which state is determined by the equilibrium constant, K_H, between the (3F)-Y_ZO^{-}---HN^{+}His and (3F)-Y_ZOH---NHis states and (2) the present data support this model.

Equation 1 relies on the assumptions that the steady-state approximation applies and that the rates of proton transfer from, k_{PT}, and to the phenol, k_{-PT}, are larger than the electron-transfer rate, k_{et}. As just discussed the satisfying correlation between the change in the activation energy induced by the fluorination and the expected change in K_H support both assumptions. In

(48) Eckert, H.-J.; Renger, G. *FEBS Lett.* **1988**, *236*, 425–431.
(49) Jeans, C.; Schilstra, M. J.; Klug, D. R. *Biochemistry* **2002**, *41*, 5015–5023.
(50) Renger, G.; Christen, G.; Karge, M.; Eckert, H.-J.; Irrgang, K.-D. *J. Biol. Inorg. Chem.* **1998**, *3*, 360–366.
(51) Tommos, C.; Babcock, G. T. *Biochim. Biophys. Acta* **2000**, *1458*, 199–219.
(52) Sjödin, M.; Irebo, T.; Utas, J. E.; Lind, J.; Merenyi, G.; Åkermark, B.; Hammarström, L. *J. Am. Chem. Soc.* **2006**, *128*, 13076–13083.
(53) Kirby, J. P.; Roberts, J. A.; Nocera, D. G. *J. Am. Chem. Soc.* **1997**, *119*, 9230–9236.

addition, the observation that the rate of the proton-coupled electron transfer through a carboxylate−guanidinium bridge was 3×10^8 s^{-1} experimentally ascertains the fact that such high rates are indeed conceivable in a H-bonded salt bridge as the one considered here.[53]

The question then arises as to the value of K_H. The mere observation that k_{app} varies with K_H shows that it cannot be much larger than 1. Yet, the acceleration, at 25 °C which results from the substitution is moderate so that K_H cannot be much smaller than 1 either. A more quantitative derivation can be made, based on eq 1. The ratio between the apparent oxidation rates of Y_Z versus 3F-Y_Z is:

$$\alpha = \frac{K_H}{K_H^F} \times \frac{(1 + K_H^F)}{(1 + K_H)} \quad (2)$$

and

$$\beta = \frac{K_H}{K_H^F} = 10^{pK - pK^F} \quad (3)$$

where, the superscript F denotes the values of K_H or pK in the case of the 3F-Y_Z. By combining eqs 2 and 3 one obtains:

$$K_H = \frac{\alpha - \beta}{1 - \alpha} \quad (4)$$

With a shift in pK_a of 1.5 pH units ($\beta = 10^{-1.5}$) and a ratio of 0.3 between the apparent rate constant for the unlabeled and labeled PSII at 25 °C, one obtains K_H (25 °C) = 0.4 (ΔG = 25 meV), which corresponds to a probability of ~0.25 for the Y_ZO^----HN^+His state (we note that this figure is, in actual fact, an overestimate, owing to the incomplete incorporation of the fluorinated tyrosine). Although present in a minority of centers, the proportion of tyrosinate state may be high enough to allow its detection by optical spectroscopy. Indeed, the difference between the (Y_Z^{ox} − Y_Z) spectra measured at pH 9.0 and 6.1 displays similarities with the deprotonation spectrum of a tyrosine.[30]

4.5. Relevance to the O_2-Evolving PSII. Finally, we believe that the above conclusions on the coupling between proton and electron transfer from Y_Z are not restricted to Mn-depleted PSII and also apply to O_2-evolving PSII. At alkaline pHs, Mn-depleted PSII shows significant kinetic similarities with O_2-evolving PSII. Indeed, the overall oxidation rate of Y_Z lies in a range similar to the one observed in O_2-evolving PSII. Furthermore, as discussed above, the activation energies of the fastest component of $P_{680}^{\bullet+}$ reduction are also comparable. The main difference thus lies in the relative weight of the components which occur in the 1−100 μs time range. It is commonly accepted that these phases, in Mn-depleted PSII, reflect heterogeneities in the H-bond network in which the phenol side chain of Y_Z is involved. Such proposals come from kinetic studies[11,21,54,55] and magnetic resonance and FTIR studies directly assessing the strength and order of the H-bonding network to $Y_ZO^{\bullet}$ or Y_ZOH.[22,30,56] Significantly, the FTIR spectra of $Y_ZO^{\bullet}/Y_ZOH$ in Mn-depleted PSII and in Ca^{2+}-depleted PSII containing the $(Mn)_4$ cluster show strong similarities.[22] In O_2-evolving PSII, the reduction of $P_{680}^{\bullet+}$ is also markedly multiphasic. The fastest component is thought to reflect the electron-transfer reaction between Y_Z and $P_{680}^{\bullet+}$, and the slow components, developing in the microsecond time range, would result from the electrostatic relaxation of the surrounding medium due to proton transfers.[57,58] Thus, although the kinetic complexity which is a common feature to Mn-depleted and O_2-evolving PSII likely stems from different causes, it seems reasonable to assume that, in Mn-depleted PSII, the fastest component probes those PSII centers in which the Y_ZOH---NHis/Y_ZO^----HN^+His state exists prior to the actinic flash. If indeed O_2-evolving PSII behaves, kinetically speaking, similarly to this subpopulation, the mechanism proposed here would apply to the active enzyme as well.

5. Conclusion

The combined use of site-directed mutants together with the global labeling by 3F-Tyr produced modifications of the driving force for electron transfer and for proton transfer from (3F)-Y_Z. The finding that the overall oxidation rate was increased with increased probability of (3F)-tyrosinate formation and was insensitive to a change in the driving force for electron transfer points to the deprotonation of the phenol group as being the determining factor in the process. Although the apparent pK_a of (3F)-YOH is significantly higher than that of the proton acceptor, *a priori* making highly unfavorable the formation of the phenolate, this deprotonation could be kinetically and thermodynamically facilitated by the H-bond network in which (3F)-Y_Z is involved as well as by the salt bridge between the phenolate and the proton acceptor. These bonds, which form at high pHs, would promote the switch from the concerted proton/electron transfer, proposed to occur at lower pHs, to the stepwise transfer of the proton and the electron from (3F)-Y_Z. This sequential transfer contrasts with the case of a phenol-carboxylate compound, which provides a H-bond to the phenol group but no salt bridge, in which a concerted proton/electron transfer was observed.[52] Significantly, this overall reaction was slower than the electron transfer from the phenolate. By fulfilling the requirements for a fast proton/electron transfer from the YO^----HN^+His ensemble, the combination of the H-bond with the phenolate−imidazolium bridge may prove more efficient as a catalyst in bioinspired photovoltaic devices as recently exemplified by a PSII-inspired construct.[59]

Acknowledgment. B.A.D. gratefully acknowledges the support of the National Research Initiative of the USDA Cooperative State Research, Education and Extension Service Grant No. 2003-35318-13589. This study was supported in part by the JSPS and CNRS under the Japan-France Research Cooperative Program (F.R., A.B., M.S.) and the Solar H program STRP from the European Union (A.B.). R.D.B. acknowledges the support of NIH, Grant No. NIH GM073789.

Supporting Information Available: Figure S1 and Table S1 describe in more detail how the simulation of the 3F-Tyr EPR spectrum was done and how the incorporation yield was quantified. Figure S2 illustrates the pH dependence of the reduction of $P_{680}^{+\bullet}$ in Mn-depleted PSII from *T. elongatus*. It

(54) Lavergne, J.; Rappaport, F. *Biochemistry* **1998**, *37*, 7899–7906.
(55) de Wijn, R.; Schrama, T.; van Gorkom, H. J. *Biochemistry* **2001**, *40*, 5821–5834.
(56) Tommos, C.; McCracken, J.; Styring, S.; Babcock, G. T. *J. Am. Chem. Soc.* **1998**, *120*, 10441–10452.
(57) Schilstra, M. J.; Rappaport, F.; Nugent, J. H. A.; Barnett, C. J.; Klug, D. R. *Biochemistry* **1998**, *37*, 3974–3981.
(58) Christen, G.; Renger, G. *Biochemistry* **1999**, *38*, 2068–2077.
(59) Moore, G. F.; Hambourger, M.; Gervaldo, M.; Poluektov, O. G.; Rajh, T.; Gust, D.; Moore, T. A.; Moore, A. L. *J. Am. Chem. Soc.* **2008**, *130*, 10466–10467.

also shows the improved quality of the fit when using four pH-independent rate constants rather than three. Figure S3 shows the high-field EPR spectra of Y_ZO° and 3F-Y_ZO° in PSII complexes from *T. elongatus* at pH 9, and Table S2 gives a summary of the geometries and hydrogen-bonding energies of the 4-ethylphenolate/imidazole, 3-fluoro-4-ethylphenolate/imidazole hydrogen-bonded supercomplexes and their respective oxidized radical versions as determined from B3LYP/6-31+G(D,P) density functional theory calculations. This material is available free of charge via the Internet at http://pubs.acs.org.

JA808604H